

---

# LEARNING DEEP MORPHOLOGICAL NETWORKS WITH NEURAL ARCHITECTURE SEARCH

---

A PREPRINT

**Yufei Hu**

U2IS, ENSTA Paris, Institut Polytechnique de Paris  
yufei.hu.2021@ensta-paris.fr

**Nacim Belkhir**

Safrantech, Safran Group  
nacim.belkhir@safrangroup.com

**Jesus Angulo**

CMM, Mines ParisTech, PSL Research University  
jesus.angulo@mines-paristech.fr

**Angela Yao**

School of Computing National University of Singapore  
ayao@comp.nus.edu.sg

**Gianni Franchi**

U2IS, ENSTA Paris, Institut Polytechnique de Paris  
gianni.franchi@ensta-paris.fr

June 16, 2021

## ABSTRACT

Deep Neural Networks (DNNs) are generated by sequentially performing linear and non-linear processes. Using a combination of linear and non-linear procedures is critical for generating a sufficiently deep feature space. The majority of non-linear operators are derivations of activation functions or pooling functions. Mathematical morphology is a branch of mathematics that provides non-linear operators for a variety of image processing problems. We investigate the utility of integrating these operations in an end-to-end deep learning framework in this paper. DNNs are designed to acquire a realistic representation for a particular job. Morphological operators give topological descriptors that convey salient information about the shapes of objects depicted in images. We propose a method based on meta-learning to incorporate morphological operators into DNNs. The learned architecture demonstrates how our novel morphological operations significantly increase DNN performance on various tasks, including picture classification and edge detection.

**Keywords** Mathematical Morphology; deep learning; architecture search.

## 1 Introduction

Over the last decade, deep learning has made several breakthroughs and demonstrated successful applications in various fields (*e.g.* in computer vision Krizhevsky et al. [2012], Simonyan and Zisserman [2014a], He et al. [2016a], Huang et al. [2017], object detection Redmon et al. [2016], or NLP Dai et al. [2019], Radford et al. [2019]). This success is mainly due to its automation of the feature engineering process. This success is mainly attributable to the fact that it automates the feature engineering process. Rather than manually designed features, features are learned in an end-to-end process from data. The need for improved architecture has swiftly followed the advent of deep learning. Experts now place a premium on architecture engineering *in lieu of* features engineering.

Architecture engineering is concerned with determining the most appropriate operations for the network, their hyper-parameters (*e.g.* the number of neurons for fully connected layers, or the number of filters or kernel size for convolutional layers), and the connectivity of all the operations. Generally, practitioners propose novel operations to validate various architectures and tasks in order to improve performance on specific tasks. As a result, developing a novel operation remains a time-consuming and costly process. It necessitates a manual search for the optimal configuration. As a result,

it is prone to failure when practitioners lack computational resources. An alternative approach focus on automatically finding the network architecture design using Neural architecture search (NAS methods) Liu et al. [2019a], Luo et al. [2019], Liu et al. [2018], Pham et al. [2018], Weng et al. [2019], Wistuba et al. [2019], Elsken et al. [2019] in lieu of a manual design. Given a set of data and a performance metric for a learning task, a NAS algorithm attempts to find the optimal architecture concerning a search strategy. It can be viewed as an optimization problem in the space of an architecture network defined by a collection of operations and their possible combinations. Recently, it was demonstrated empirically on several applications that architectures discovered using NAS outperform those discovered manually.

Recently, we have observed a steady increase in interest in mathematical morphology amongst the deep learning community. Indeed, the intrinsic features of mathematical morphology operators that enable them to extract information from topological structures make them excellent candidates. Morphological operators have been shown to capture image edges Rivest et al. [1993], granulometry Serra [1988], Thibault et al. [2013] and distances to object borders Franchi and Angulo [2014]. Two methodologies are employed in the literature to evaluate the utility of morphological operators. Some analyses Cavallaro et al. [2017], Velasco-Forero and Angulo [2013], Franchi and Angulo [2016] directly extract descriptors from unlearned morphological layers, while others Franchi et al. [2020], Valle [2020], Mondal et al. [2020] propose learning the structural element of the morphological operators. Despite their superior performance in various application situations, these methodologies are prone to failure if the deep network architecture is misdesigned, which may dissuade researchers from pursuing this research path.

This paper proposes a novel methodology based on neural architecture search to assess the usefulness of newly developed architecture layers and, in particular, morphological layers. The following paper empirically investigates morphological layers applied to deep networks on CIFAR10/CIFAR100 Krizhevsky [2009] and an edge detection task using BSD500 Martin et al. [2001], to determine the optimal design for morphological layers. We compare our results to the best architecture discovered using conventional convolutional layers.

Our contributions can be summarized as follows:

- First, we propose novel procedures based on sub-pixel convolutions and mathematical morphology to construct pseudo-morphological operations using standard convolution layers.
- We integrate these procedures into deep networks using morphological layers and NAS algorithms. We demonstrate empirically that our architecture tailored to morphological layers can outperform conventional convolutional layers.
- We outline some current issues in NAS and introduce the problem of choosing the backbone, *i.e.* the higher-level architecture design on which the search will be performed. We offer novel network space descriptions suitable for the edge identification job.
- We are the first to examine architectural search mixed with morphological procedures for edge detection. Our new specialized architecture achieves state-of-the-art performance for edge detection.

## 2 Related work

### 2.1 Mathematical Morphology

Mathematical morphology has been extensively used to denoise raw images Serra [1983]; it has also been used to characterize and analyze microscopic images Boizeau et al. [2013], Franchi et al. [2018], Drouyer et al. [2017], and remote sensing Franchi and Angulo [2016, 2014], Cavallaro [2016], Cavallaro et al. [2017], Fauvel et al. [2007], Benediktsson et al. [2003], Velasco-Forero and Angulo [2013]. Additionally, these operators have been used to generate medical images Dufour et al. [2013], Zhang et al. [2012]. However, all of these morphological paper operators were used as filters to derive feature descriptors from the classifier’s input data. We decided to integrate them into a Deep Neural network in this case.

### 2.2 Morphological neural network

Masci et al. Masci et al. [2013] pioneered the use of morphological operators in neural networks. They began researching pseudo harmonic morphological operators in conjunction with DNNs. First morphological Perceptrons has been investigated in Saeedan et al. [2018], Zhang et al. [2019], Mondal et al. [2019], Valle [2020], Charisopoulos and Maragos [2017]. Some investigations attempted to integrate morphological layers and DNN architecture Mellouli et al. [2017], Mondal et al. [2020], Franchi et al. [2020], Nogueira et al. [2019]. The issue with these works is that one could argue that morphological procedures are architecture-dependent. As a result, we propose in our work to link the search

for architecture using morphological layers. Let us disregard the work of Blusseau et al. Blusseau et al. [01 Jan. 2020], who used auto-encoder networks to approximate morphological operators.

### 2.3 Neural Architecture search

Experts in the machine learning field typically create deep neural networks by hand and pick hyper-parameters through a trial-and-error process. As a result, the process becomes tiring and tedious, as well as prone to errors. A different perspective sees model design as a decision-making process that can be improved. We can automatically find the best combination of algorithms to maximize the performance of a task. With the growing interest in deep learning, AutoML Zöller and Huber [2019], Zoller and Huber [2020] and Neural architecture search Wistuba et al. [2019] emerged where the entire DL pipeline could be automated, with the expectation to reduce the overall development cost and approach experts performances. There has been several efforts Zoph and Le [2016], Floreano et al. [2008], Ren et al. [2020], Pham et al. [2018], tracing back to the 90's Kitano [1990], Miller et al. [1989], formulating NAS as an optimization in the space of network architectures and solved using either reinforcement learning algorithms Pham et al. [2018], Liu et al. [2019b], gradient-based optimization Liu et al. [2019a] or sequential model-based optimization Liu et al. [2019b], Camero et al. [2020].

## 3 Morphological Architecture Search (MAS)

We first outline some preliminaries on the convolution operation and its relationship to mathematical morphology in Sec. 3.1. We then outline our proposed pseudo-morphological dilation operation (Sec. 3.2) and the variants in (Sec. 3.3). We then explain the architecture search algorithm that we use to integrate the operators into a neural network (Sec. 3.4). Finally, describe the proposed architecture backbone.

### 3.1 Preliminaries

Consider a discrete RGB image  $f$ , where  $f[i, j, 0]$ ,  $f[i, j, 1]$ ,  $f[i, j, 2]$  denotes the red, green, and blue values at position  $(i, j)$ . We further denote as  $g$  the feature map resulting from a DNN's convolution layer of  $f$  with the filter  $\omega$  without bias. The feature map  $g$  can be expressed as

$$g[n_1, n_2, c] = \sum_{k=0}^2 \sum_{(i,j) \in \mathcal{N}} f[n_1 + i, n_2 + j, k] \omega[i, j, k] + b[c], \text{ with } c \in [1, C_{\text{out}}] \quad (1)$$

where  $\mathcal{N}$  is a square kernel that defines the spatial size of the convolution kernel,  $c$  is the index of the channel, and  $C_{\text{out}}$  is the number of channels output of the layer, and  $b$  is the bias equal to zeros if we consider the unbiased convolution. In this case, we consider the convolution with a bias  $b$ , then  $g$  can be expressed as

By analogy, mathematical morphology Serra [1983] operators are non-linear image operators based on the spatial structure of the image. First, these operators were proposed for binary images; now, they have been extended for grayscale images. Let  $f$  be a grayscale image representing a function, with the intensity at position  $x$ , denoted as  $f(x)$ . The two basic operations in morphology are performed at the grey level, such that we define the erosion and dilation operations on their discrete version respectively as:  $\varepsilon_b(f)[n_1, n_2] = \min_{(i,j) \in \mathcal{N}} f[n_1 + i, n_2 + j] - b[i, j]$  and  $\varepsilon_b(f)[n_1, n_2] = \max_{(i,j) \in \mathcal{N}} f[n_1 - i, n_2 - j] + b[i, j]$  where  $b = [b_{-n}, \dots, b_n]$  is a structuring element (SE). In Figure 1, we observe that the dilation increases the bright areas based on the shape of the SE leading to a brighter image. Erosion is the morphological dual to dilation and will decrease the bright areas. We can see a direct link between the dilation erosion and convolution where the dilation is a convolution in the max + algebra as explained in Angulo [2017].

These operations are increasing hence:  $f < g \Rightarrow \varepsilon_b(f)(x) < \varepsilon_b(f)(x)$  or  $f < g \Rightarrow \delta_b(f)(x) < \delta_b(f)(x)$ . In addition, the erosion is anti-extensive, while the dilation is extensive hence:  $f \geq \varepsilon_b(f)(x)$  and  $\delta_b(f)(x) \geq f$ .

By combining these two basic operations, we can build new ones such as the opening and closing. The opening of image  $f$  by structuring element  $b$  is given by applying an erosion on  $f$  with the structuring element  $b$  and then applying a dilation on the previous results with the same SE. The closing operation is the morphological dual to the opening.

$$\gamma_b(f) = \delta_b(\varepsilon_b(f)), \text{ and } \varphi_b(f) = \varepsilon_b(\delta_b(f)). \quad (2)$$

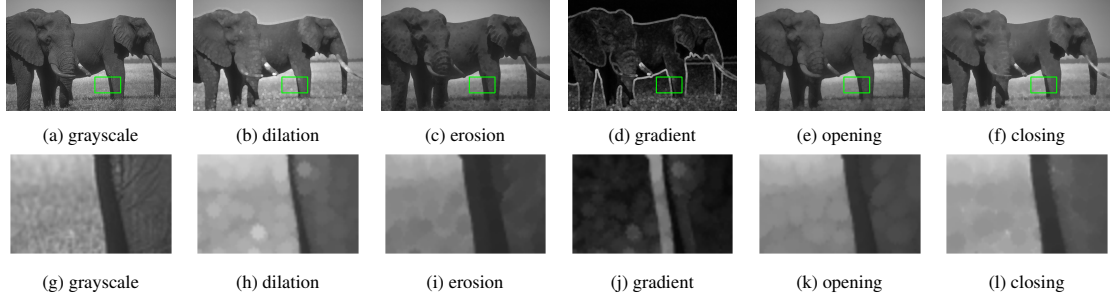


Figure 1: Dilation and erosion transformation where the structuring element is disk(3) applied on a sample image from the BSD500 dataset Arbelaez et al. [2011].

By combining these two basic operations, we can also build the internal gradient, the external gradient denoted respectively  $G_i$  and  $G_e$  and defined as:

$$G_e(f) = \delta_b(f) - f, \text{ and } G_i(f) = f - \varepsilon_b(f) \quad (3)$$

In addition, we can also build the morphological gradient which is the difference between the dilation and the erosion with the same SE applied on the same image. Hence it is defined as:  $G_b(f) = \delta_b(f) - \varepsilon_b(f)$  The structuring element impacts morphological operations by both the geometry of its support and its weights. Hence, by combining morphological operators, we can build new operators. One could wonder how to combine these operators to have the best performances for a given task. For a while, these operators were combined based on expert knowledge. In this work, we propose to combine them, thanks to an architecture search algorithm.

### 3.2 Our pseudo-morphological dilation

We propose the bfpseudo morphological dilation operation. This operation is composed of the following step:

1. We apply a traditional convolution operation to transform the feature map form  $(C, H, W)$  into  $(C \times r \times r, H, W)$  where  $r$  represents the size of the convolution kernel,  $H$  and  $W$  represents respectively the height and width of the image. Hence, we increase the number of feature map channels. Each feature map represents a neighborhood map that will be used in the step. For example, in Figure 2a, we have four feature maps. We denote this step the **Projection convolution step**. Let us denote  $f$  the input image and  $\omega$  the convolution kernel of spatial size  $1 \times 1$  and  $b$  the bias of the projection convolution. Let us consider that the convolutional layer has  $C_{\text{in}}$  input channels and  $C_{\text{out}}$  output channels. Hence, the resulting feature map at pixel  $n_1, n_2$  is equal to:

$$g[n_1, n_2, c] = \sum_{k=0}^{C_{\text{in}}} f[n_1, n_2, k] \omega[0, 0, k] + b[c], \text{ with } k \in [1, C_{\text{out}}] \quad (4)$$

2. We then apply the Pixel Shuffle transformation to the feature maps representing coordinates as illustrated in Figure 2b. Pixel Shuffle transformation, also known as sub-pixel convolution, was introduced Shi et al. [2016] for the super-resolution task. The Pixel Shuffle transformation reorganizes the low-resolution image channels to obtain a bigger image with fewer channels. Specifically, it increases the spatial size of the feature map by reducing the number of channels. Hence it rearranges the input tensor elements expressed as  $(C \times r \times r, H, W)$  to form a scaled  $(C, H \times r, W \times r)$ . This operation is interesting since it is stable, compatible with deep learning back propagation, and does not add any artifacts. We denote this step the **Pixel Shuffle step**. More formally, each channel  $c$  of the previous step represents a neighborhood as illustrated in Figure 2. Let us decompose equation 4 in two terms such that for all  $c$  we have  $g[n_1, n_2, c] = \tilde{f}[n_1, n_2, c] + b[c]$  where  $\tilde{f}$  is the results of the cross correlation of the convolution layer. Note that  $C_{\text{out}} = r^2 C_{\text{in}}$ . The output of pixel shuffle is :

$$h[n_1, n_2, c] = g[\lfloor n_1/r \rfloor, \lfloor n_2/r \rfloor, c'] \quad (5)$$

where  $\lfloor n_1/r \rfloor$  is the floor fraction: it takes as input a real number  $n_1/r$  and outputs the greatest integer value. The channel  $c'$  is equal to  $c' = c + n_1 \cdot \text{mod}(r) + n_2 \cdot \text{mod}(r) + r \mathbf{1}_{n_2 \cdot \text{mod}(r) > 0}$ , where  $\text{mod}(r) = n_1 - (\lfloor n_1/r \rfloor \times r)$ .

3. On the output of the Pixel Shuffle step we apply a max-pooling of stride  $r$ . We denote this step the **Max-pooling step**. We apply the max pooling into  $h$  with kernel of spatial size of  $r \times r$  and a stride  $r$ , let us denote  $h'$  the result. Then  $h'$  is equal to :

$$h'[n_1, n_2, c] = \max_{(i,j) \in \mathcal{N}} f[\lfloor (n_1 + i)/r \rfloor, \lfloor (n_2 + j)/r \rfloor, c'[i,j]] + b[c'[i,j]] \quad (6)$$

where  $c'[i, j] = c + (n_1 + i).\text{mod}(r) + (n_2 + j).\text{mod}(r) + r\mathbf{1}_{(n_2 + j).\text{mod}(r) > 0}$ . So we ended having a dilation on  $\tilde{f}$  where the bias  $b$  is the structuring element, with a connectivity depending on the channel.

Classical morphological operators can be hard to train due to the non linearity, as pointed out in Franchi et al. [2020], where the authors proposed to clip the gradients of these layers and apply specific learning on these layers. Hence integrating them into a NAS framework can be challenging, this is due to the fact that NAS framework will try to learn the best architecture with the set of operations. So we cannot build a hand-designed architecture that will stabilize the new layers. Hence the new layers must be stable to any architecture. So we proposed a stable version that we are going to introduce in this section.

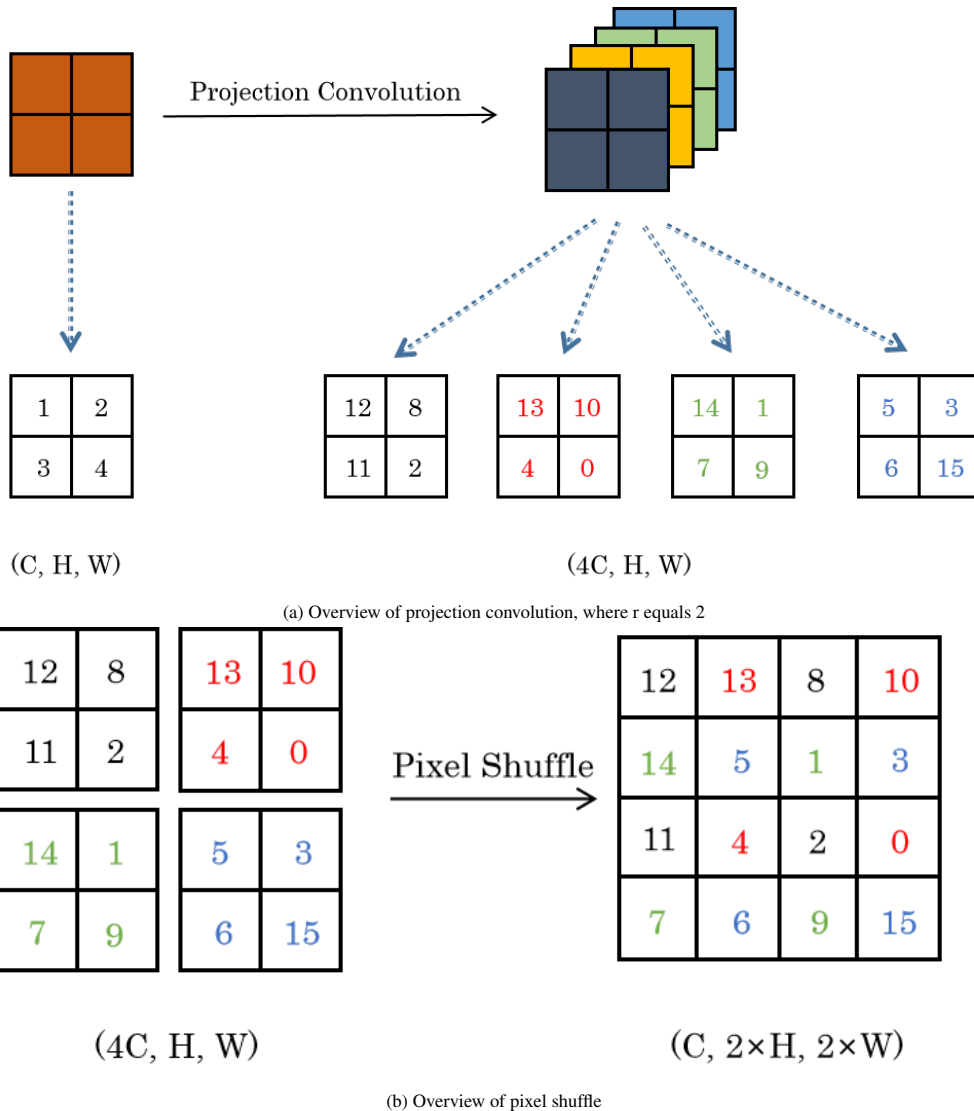


Figure 2: A simple example to explain the projection convolution and pixel shuffle step. We start with a feature map composed of 4 pixels of value (1,2,3,4), then we apply the projection convolution have four feature maps of value (12,8,11,2),(13,10,4,0),(14,1,7,9) and (5,3,6,15). Then by applying the pixel shuffle, we have just one feature map.

The full layer is represented in the diagram of Figure 3. We simulate the structuring element's shape by working with the parameter  $r$  of the max pooling and the pixel shuffle layer. We notice that by adding a Batch Normalisation Ioffe

and Szegedy [2015] before the **Projection convolution step**, the results were more stable. Hence, we used it on all our layers. We denote this layer as a pseudo dilation because it is not an increasing function nor an extensive function between the input and the output. Still, it checks these properties between the input and output of the max pooling.

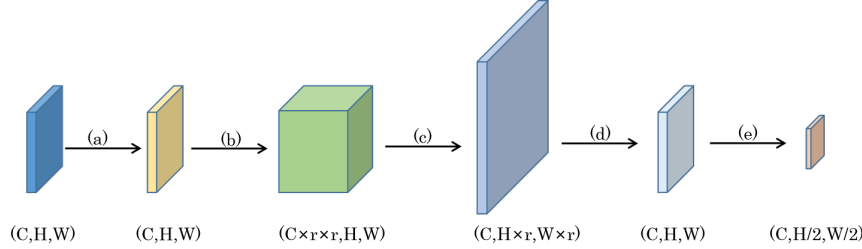


Figure 3: The overview of **pseudo morphological dilation, pool and erosion**. The transformation are composed of 4 steps mandatory (a),(b),(c),(d) and one optional step (e). (a) is a Batch normalisation to transform the input feature maps.(b) Traditional convolution to transform the feature map from  $(C, H, W)$  into  $(C \times r \times r, H, W)$ . (c) is a Sub-Pixel convolution that makes the length and weight of feature map expanded by  $r$  times. (d) max-pooling or a min-poling if we perform a dilation or an erosion respectively that makes the output feature map dimension consistent with the input feature map. (e) is an optional max-pooling operation with a stride of 2.

### 3.3 Our morphological layers

Based on the description of our pseudo morphological dilation, which is our base operators, we will describe four more operators in this sub-section. Namely, these operators are: the **pseudo morphological erosion**, the **pseudo morphological pooling**, the **pseudo morphological upsampling**, and the **pseudo morphological gradient**.

The **pseudo morphological erosion** is constructed with the same exam step as the **pseudo morphological dilation** except that instead of doing a max-pooling after the pixel shuffle step, we apply a min-pooling. We proposed this operation to check the usefulness of such an operation based on the minimum. We illustrated this layer in as shown in Figure 3.

Similarly to convolution layers with stride, we proposed **Pseudo morphological pooling**. This operation consists of applying first a pseudo morphological dilation operation followed by an extra max-pooling as shown in Figure 3. In other words, we achieved downsampling by this approach of the input image.

We propose for edge detection task **pseudo morphological upsampling** which is similar to a deconvolution layer. This operation is implemented by transforming the feature map from  $(C, H, W)$  to  $(r^2 \times s^2 \times C, H, W)$  through the **Projection convolution step**. Then we apply the **Pixel Shuffle step** to form feature maps with the size of  $(C, r \times s \times H, r \times s \times W)$ . Subsequently we apply the **Max-pooling step** with stride  $r$ .

We propose a new layer called the **pseudo morphological gradient**. For this layer, we achieve the same **Projection convolution step**, and **Pixel Shuffle step**. Then we get pseudo morphological dilation feature maps using max-pooling, and we get the final gradient feature map by performing vector subtraction with the input image. Contrary to the morphological gradient which is positive for all pixels, this one is not necessarily positive. This is also happening with the morphological Laplacian Serra [1988] that is interesting to denoise images. Also, the skip connection provided by this gradient layer can help to avoid vanishing gradients. This layer is illustrated in Figure 4.

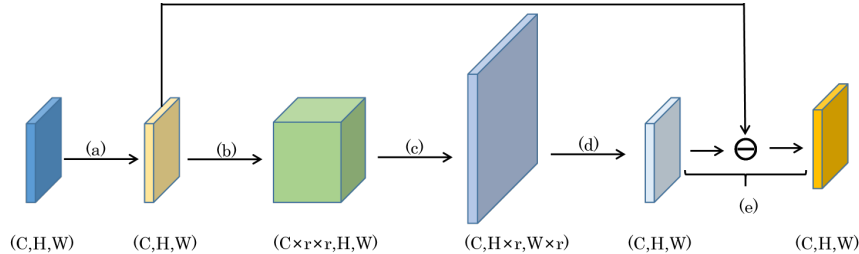


Figure 4: The overview of **pseudo morphological gradient** The process of (a)(b)(c)(d) is same with pseudo morphological dilation. (e) the vector subtraction to get the external pseudo gradient.

### 3.4 Neural Architecture Search (NAS)

Neural Architecture Search (NAS) Liu et al. [2019a], Luo et al. [2019], Liu et al. [2018], Pham et al. [2018], Weng et al. [2019], Wistuba et al. [2019], Elsken et al. [2019] has recently identified neural network architectures that exceed human-designed ones on large-scale image classification Liu et al. [2019a], Luo et al. [2019], Liu et al. [2018], Pham et al. [2018]. As illustrated in Figure 5, NAS need three key elements :

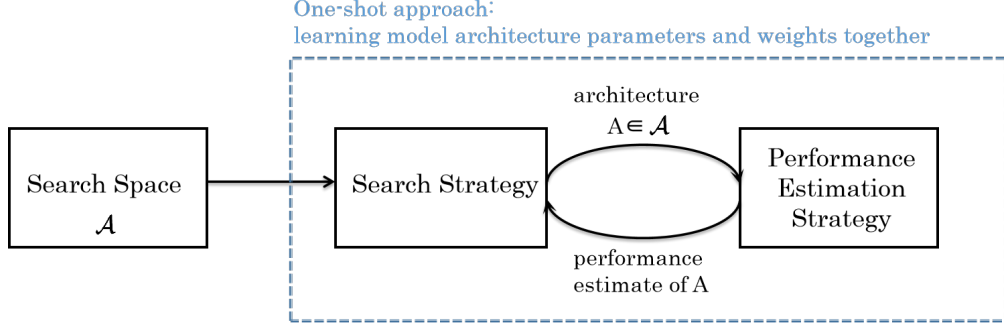


Figure 5: Components of Neural Architecture Search(NAS) model

1. **Search Space:** which defines a set of operations (e.g. convolution, fully-connected, pooling) and how we want them to be connected to build valid network architectures. In some sense, the search space defines the space of admissible solution.
2. **Search algorithm:** which is the algorithm used to optimise the architecture
3. **Criterion:** which defines the measure to estimate or predict the performance of an architecture.

The **criterion** used for all the different tasks is the accuracy criterion applied to the validation; we want to optimize for the given task. On the rest of this section, we will describe our **search space** and our **search algorithm**.

#### 3.4.1 Search space- Cell search

In the NAS community, the search space represents the space where we search the DNN's architecture. Thanks to a set of operations and a backbone explaining how operations can be connected to construct valid network architectures, it is defined thanks to a set of operations and a backbone. The search space can be classified into two categories. The first one is the **Global Search Space** where the algorithm has to learn all the DNN architecture. The second one is the **Cell-Based Search Space** where the DNN architecture lies in a backbone composed of basic components called cells, and the goal is to learn what is inside the cells. Inspired by DNN architecture such as ResNet He et al. [2016b], VGG Simonyan and Zisserman [2014b], and Inception Szegedy et al. [2017], the author of NASNET Zoph et al. [2018], who initially proposed cell-based search space, noticed that a DNNs are composed of blocks with the same kind of operations that are repeated multiple times. In Figure 6, we represented the backbone of DNN model for CIFAR10 Krizhevsky [2009].

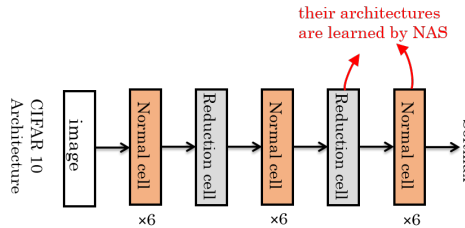


Figure 6: The overall backbone of Cell-Based CNN model for CIFAE 10.

The Cell-Based Search Space appears to be a more popular alternative than Global Search Space because the newly discovered neural architecture based on Cell-Based Search Space can be easily transferred between datasets. Two sorts of cells are commonly employed for classification. The first is the standard cell, which preserves the feature map's spatial size, and the second is the reduction cell, which shrinks the feature map's spatial size.

Cell search space without morphological layer	Cell search space with dilation	Cell search space with erosion
	separable conv $3 \times 3$	
	separable conv $5 \times 5$	
	average pooling	
	maximum pooling	
$\emptyset$	pseudo morphological dilation $3 \times 3$	pseudo morphological erosion $3 \times 3$

Table 1: Cell search space for the classification task. separable conv  $3 \times 3$  and separable conv  $5 \times 5$  are the separable convolutions introduced in Chollet [2017] with a kernel size of  $3 \times 3$  and  $5 \times 5$ .

Cell search space without morphological layer	Cell search space with dilation	Cell search space with erosion
	cweight $3 \times 3$	
	separable conv $3 \times 3$	
	conv $3 \times 3$	
	average pooling	
	maximum pooling	
separable conv $5 \times 5$	pseudo morphological dilation $3 \times 3$	pseudo morphological gradient $3 \times 3$

Table 2: Cell search space for the edge detection task. cweight  $3 \times 3$  is a the Squeeze-and-Excitation Networks(SENet) introduced in Luo et al. [2019] with a kernel size of  $3 \times 3$ .

### Cell search space for classification

We tested three cell search spaces for the classification task, two with the morphological layer and one without. The different search spaces are illustrated in Table 1.

### Cell search space for edge detection

For the edge detection task, we proposed three cell search spaces composed of 6 operations. To study pseudo morphological operation's influence, all the search spaces have the same number of operations. The different search spaces are illustrated in Table 2.

#### 3.4.2 Search space of Architecture

As illustrated in Figure 6, the search architecture space is a backbone designed by repeating multiple modules composed of reduction cells and normal cells for classification. For the task classification, we did not change the search architecture space. However, we proposed search architecture space for segmentations where the DNNs play with multiple resolutions, skip connections, and deconvolution.

**U-Net Architecture search space** The U-Net architecture Ronneberger et al. [2015] inspired our first search architecture space, that we denote U-Net search space. We started with this search space since U-Net has state-of-the-art for medical images.

The U-Net architecture is a fully convolutional network that reinjects the decoder feature map from the encoder information. Hence the spatial information might be more precise.

Our U-Net search space backbone is similar to the U-Net DNN backbone. However, it is composed of two types of cell: downsampling segmentation cell and upsampling segmentation cell, which we denote DownSC and UpSC. The upsampling segmentation cell is composed of the following operations:

- separable conv  $3 \times 3$
- separable conv  $5 \times 5$
- average pooling
- maximum pooling
- pseudo morphological gradient  $3 \times 3$
- transpose convolution

The overall U-Net search backbone is shown as the Figure 7 following.

### Multi-scale decoder Architecture search space

Inspired by DeepLab V3+ Chen et al. [2018], PSPNet Zhao et al. [2017], and RCFLiu et al. [2019b], we notice that a good architecture for general images relies on an encoder pretrained on ImageNetRussakovsky et al. [2015] and a

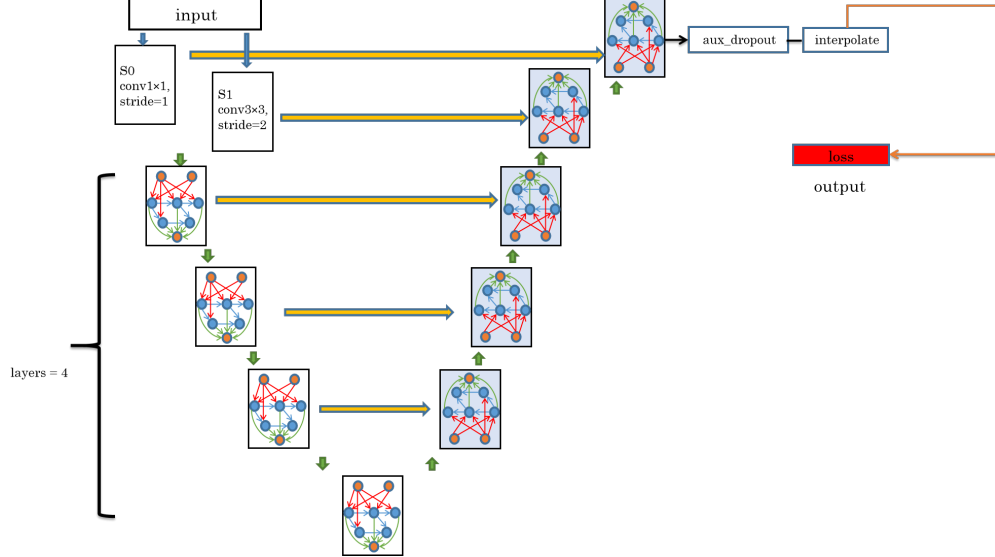


Figure 7: The overall backbone of Cell-Based U-netRonneberger et al. [2015]Weng et al. [2019], where  $C$  equals 8,  $B$  represents the number of intermediate nodes,  $H_0$  equals  $0.25H$ ,  $H_1$  equals  $0.5H_0$  and the rest can be done in the same manner. Similarly, the value of  $W$  is derived in the same way. In addition, the  $aux\_dropout$  is a operation sequential.

decoder that takes as input multiple resolutions and associate them to build the output. Based on that we propose our new network search space that we denote Multi-scale decoder search network space.

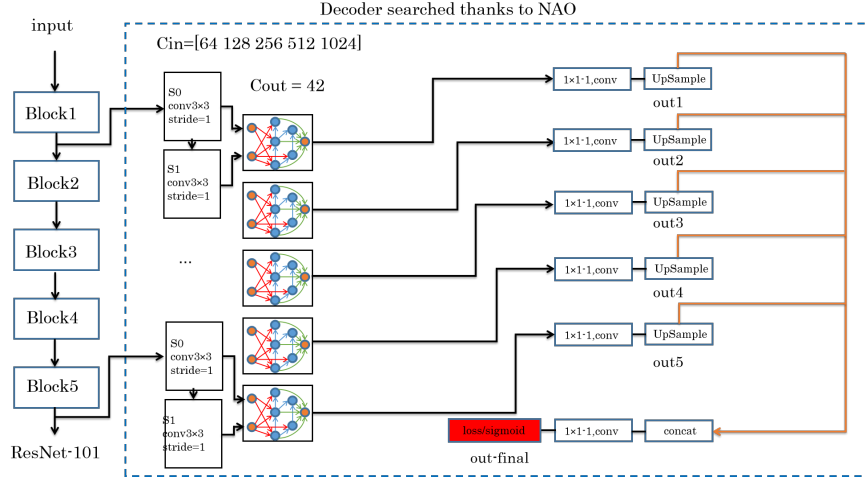


Figure 8: ResNet101\_Decoder

Our new network search space illustrated in Figure 8 can be summarized as follows. We use a ResNet architecture He et al. [2016b] pretrained on ImageNetRussakovsky et al. [2015] as an encoder network similarly to Chen et al. [2018], Zhao et al. [2017], Liu et al. [2019b]. ResNet is composed of 4 blocs. We connected each block's output to two layers. The first one is a preprocessing layer that we denote  $S_0$ . This layer is composed of a  $3 \times 3$  convolution and output 42 feature maps. This operation allows us to control the depth map that will enter the cells. The second preprocessing applied on the output of  $S_0$ , and denoted  $S_1$ , is composed of a  $3 \times 3$  convolution and outputs 42 feature maps. The input of the cells are the output of  $S_0$  and  $S_1$ , so that the cell learns if it wants to use  $S_0$  or/and  $S_1$ . After each block, We use a  $1 \times 1$  convolution on the cells' output to reduce the channel's number to one. This convolution is followed by an upsampling to resize all the feature maps to input size and we concatenate all upsampled results. Finally, we use a  $1 \times 1$  to produce the final edge detection map.

### 3.4.3 Neural Architecture Optimization (NAO)

NAO Luo et al. [2019] is an optimization algorithm that searches the best architectures based on the following principle. First, NAO is a **Cell-Based Search Space** algorithm like most modern NAS. Hence we just need to learn the adjacency matrix that represents the cells. Secondly, NAO is a **two-step algorithm** that first searches the best architecture in *step 1*. Then, in *step 2* with this architecture, NAO optimizes the DNN's weights to search for the best model. Thirdly, NAO does not directly optimize the cell parameters, and it performs its optimization on a **latent space** of cell parameters.

NAO process is illustrated in Figure 9. In detail, The NAO algorithm consists of an encoder, a predictor, and a decoder networkLuo et al. [2019]. The encoder of NAOLuo et al. [2019] takes an architecture sequence randomly generated describing an architecture as input, and then maps it into a continuous space C. Specifically, the encoder is denoted as  $E : X \rightarrow C$ . Let us write  $e_x = E(x)$  the latent representation of the DNN architecture.

The performance predictorLuo et al. [2019]  $P : C \rightarrow R$  maps the latent representation of an architecture  $x$  into its performance  $s_x$ . For an architecture  $x$  and its performance  $s_x$  as training data, the optimization of  $P$  aims at minimizing the least-square regression loss  $= (s_x - P(E(x)))^2$ .

The decoder of NAOLuo et al. [2019], which is similar to the decoder in the DNN model, the decoder in NAO is responsible for decoding out the string tokens in  $x$ , taking  $e_x$  as input. Mathematically the decoder is denoted as function  $D : C \rightarrow X$  which decodes the input taking  $e_x$ . The training process consist of optimizing the following loss :  $\sum_{x \in X} \log P_D(x | E(x))$ .

The Encode-Decoder will learn to build a latent space that can represent the space of architecture. The performance predictor learns to map this space to its performance for the given task. Finally, they generate new architecture by trying to find the one that has the best performance.

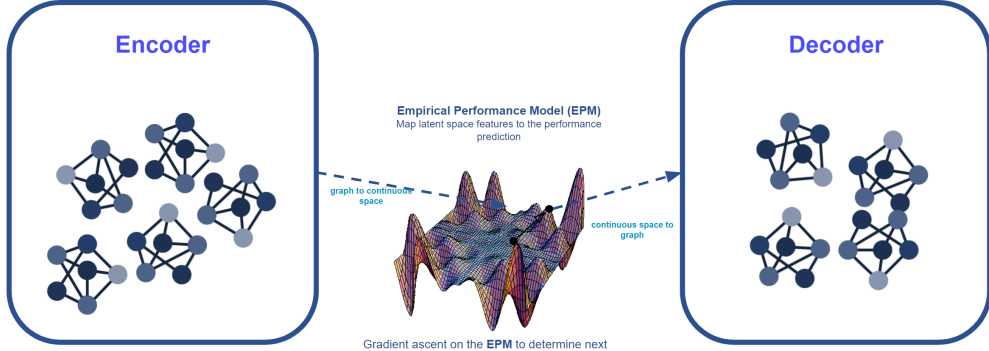


Figure 9: Overview of NAO algorithm. The encoder maps architecture  $x$  into a continuous space represented by  $e_x$ . Afterwards, the predictor optimizes  $e_x$  by maximizing the output of performance using gradient descent. And the output of predictor is represented as  $e_{x'}$ . The decoder transforms  $e_{x'}$  into a new discrete architecture  $x'$ Luo et al. [2019]

## 4 Experiments

In this section, we will explain the experiments confirming our morphological layers' utility. We looked at two different types of experiments: classification and edge detection.

### 4.1 Classification task

We evaluated our layers on two datasets : CIFAR10Krizhevsky [2009] and CIFAR100Krizhevsky [2009]. CIFAR10 and CIFAR100 are two data set composed of 50 000 training RGB images and 10 000 RGB test images. The Images are of size  $32 \times 32$ . CIFAR10 has 10 classes, while CIFAR100 has 100 classes. To train the DNN, we used the cross-entropy loss and reported the classification error. To train the DNN, we use the same experimental protocol as NAO use for CIFAR 10. During the architecture search, we use a small network with  $B = 5$  (number of nodes),  $N = 3$  (number of normal cells),  $F = 8$  (number of channels) and search the architecture for four iterations; each of them is composed of 50 epochs. After the best cell architectures are found, we increase the architecture with  $B = 5$ ,  $N = 6$ ,  $F = 36$  and optimize the weight of the DNNs for 600 epochs. The batch size for the two-step is 128. The results in Table 3 are the mean of 3 seeds. The mean error of our architecture with the morphological layer is 2.65%, which is below 2.93% of NAOLuo et al. [2019]. We tried to replace the morphological dilation with erosion and saw that the result decreased.

Hence we noticed on CIFAR 10 that the morphological dilation layer improves the performances of the DNN. We also noticed from Figure 10 that NAO used this operation since it is present in 3 edges out of 15 for the Normal Cell and 4 out of 15 for the Reduction Cell. Morphological operations seem to bring information not present by traditional convolutional that can help to improve performances.

We have illustrated in Figure 10 the normal and reduction cell structure that we learned for the CIFAR10 Krizhevsky [2009] classification task. As one can see the cells are represented by a graph, which can be characterized by an adjacency matrix that we are drawn in Figure 11.

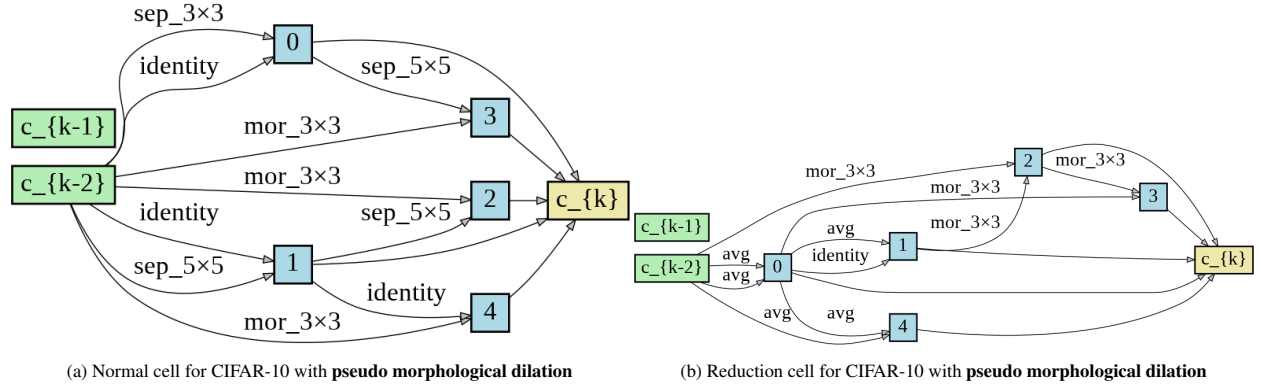


Figure 10: Cell structure for the classification of CIFAR10, where  $c_{k-1}$  represents the previous output.  $c_{k-2}$  represents the output of the cell just before  $c_{k-1}$ . The blue number 0-4 represent the intermediate nodes and every edge represents different operations. In addition,  $c_k$  represents the output of the current cell which concatenates the results of intermediate node 0-4.

$$\begin{array}{ccccccccc}
& c_{k-1} & c_{k-2} & n_0 & n_1 & n_2 & n_3 & n_4 & c_k \\
\begin{array}{c} c_{k-1} \\ c_{k-2} \\ n_0 \\ n_1 \\ n_2 \\ n_3 \\ n_4 \\ c_k \end{array} & \left[ \begin{array}{ccccccc} 0 & 0 & 0 & 0 & 0 & 0 & 0 & 0 \\ 0 & 0 & (1,5) & (2,5) & 6 & 6 & 6 & 0 \\ 0 & (1,5) & 0 & 0 & 0 & 0 & 0 & 7 \\ 0 & (2,5) & 0 & 0 & 0 & 0 & 0 & 7 \\ 0 & 6 & 0 & 2 & 0 & 0 & 0 & 7 \\ 0 & 6 & 2 & 0 & 0 & 0 & 0 & 7 \\ 0 & 6 & 0 & 5 & 0 & 0 & 0 & 7 \\ 0 & 0 & 7 & 7 & 7 & 7 & 7 & 0 \end{array} \right] & \begin{array}{c} c_{k-1} \\ c_{k-2} \\ n_0 \\ n_1 \\ n_2 \\ n_3 \\ n_4 \\ c_k \end{array} & \left[ \begin{array}{ccccccc} 0 & 0 & 0 & 0 & 0 & 0 & 0 & 0 \\ 0 & 0 & (3,3) & 0 & 6 & 0 & 3 & 0 \\ 0 & (3,3) & 0 & 0 & 0 & 0 & 0 & 7 \\ 0 & 0 & (3,5) & 0 & 0 & 0 & 0 & 7 \\ 0 & 6 & 6 & 0 & 0 & 0 & 0 & 7 \\ 0 & 0 & 6 & 0 & 6 & 0 & 0 & 7 \\ 0 & 0 & 6 & 0 & 6 & 0 & 0 & 7 \\ 0 & 0 & 7 & 7 & 7 & 7 & 7 & 0 \end{array} \right] \end{array}$$

Figure 11: The adjacency matrix for normal cell and reduction cell. From left to right: the adjacency matrix of normal cell, the adjacency matrix of reduction cell. Among them, the number 1,2,3,4,5,6, and 7 represent respectively the following layers : separable conv  $3 \times 3$ , separable conv  $5 \times 5$ , avg pool, max pool, identity, pseudo morphological dilation  $3 \times 3$ , and concatenate operation respectively.

We also trained an architecture search on CIFAR100 and checked that we could confirm our previous result. We can see in Table 4 our results for CIFAR100. We notice that the morphological layer seems to improve the performances of the classification task. We also noticed that training from scratch on the architecture search on CIFAR100 bring worse results than transferring the architecture learned on CIFAR10.

## 4.2 Edge detection task

We offer a method for extracting image edges to highlight the power of morphological operators in deep learning frameworks. We recommended two backbones for this task. Both the U-Net search backbone and the Multi-scale decoder Architecture search space are detailed in the section 3.4.2.

Method	B	Error(%)
ResNet with stochastic depthHuang et al. [2016]		5.25
Wide ResNetZagoruyko and Komodakis [2017]		4.00
ENAS+CutoutPham et al. [2018]	5	3.54
Block-QNN-S more filtersZhong et al. [2018]		3.54
DenseNet-BCHung et al. [2018]		3.46
PNAS+CutoutLiu et al. [2018]	5	3.41
DARTS+CutoutLiu et al. [2019a]	5	2.83
NAONet-WSLuo et al. [2019]	5	3.53
NAONet-WS+CutoutLuo et al. [2019]	5	2.93
NAONet-WS+Cutout+ <b>pseudo morphological dilation</b>	5	<b>2.65</b>
NAONet-WS+Cutout+ <b>pseudo morphological erosion</b>	5	3.20

Table 3: CIFAR10 Performance of NAONet with pseudo morphological operations, where B represents the number of nodes within the cell. Error represents the accuracy error.

Method	B	Error(%)
ResNet with stochastic depthHuang et al. [2016]		24.98
Wide ResNetZagoruyko and Komodakis [2017]		19.25
Block-QNN-S more filtersZhong et al. [2018]		18.06
PNAS+Cutout*Liu et al. [2018]	5	17.44
DenseNet-BCHung et al. [2018]		17.18
ENAS+Cutout*Pham et al. [2018]	5	16.44
NAONet-WS+Cutout*Luo et al. [2019]	5	<b>15.67</b>
NAONet-WS+Cutout+ <b>without pseudo morphological dilation</b>	5	16.9
NAONet-WS+Cutout+ <b>pseudo morphological dilation</b>	5	<b>16.23</b>

Table 4: CIFAR100 Performance of NAONet with pseudo morphological operations, where B represents the number of nodes within the cell. Error represents the accuracy error. Please note that the results of the techniques with a star \* trained the architecture search on CIFAR10 and learn the model on CIFAR 100.

We trained our DNNs on BSDS500 Arbelaez et al. [2011], which comprises 200 training, 100 validation, and 200 test images. Up to 9 annotators labeled each image. Like previous works Liu et al. [2019b], Liu and Lew [2016], Yang et al. [2016], Kokkinos [2015], we used the training set and validation set for tuning the DNN and test set for evaluation and mixed the augmented training data of BSDS500 with flippedVOC Context dataset Mottaghi et al. [2014].

On medical images, U-Net backbone has state-of-the-art performance for semantic segmentation, yet as illustrated in Table 5 this backbone does not have good results for edge detection. Then we proposed a Multi-scale decoder Architecture search space that we denote **NAO-Multi-scale**. This backbone is inspired by Traditional algorithmsWen et al. [2018] that perform well on this task. This algorithm learns a decoder using an encoder pre-trained on ImageNetRussakovsky et al. [2015].

To evaluate our novel algorithm, we use the F1-score. The F1-score is the harmonic average of the precision and recall and ranges between 0 and 1, with higher values being better. We evaluate the F1 score for each image of the test set of BSDS500Arbelaez et al. [2011] at different thresholds for the edge prediction. We apply different thresholds since our results are edge probabilities with values between zero and one. The closest to 1 the edge value is, the more probable this edge is correct. Yet this metric does not provide a result for all the dataset. Hence similarly to papers Liu et al. [2019b], Liu and Lew [2016], Yang et al. [2016], Kokkinos [2015] the Optimal Dataset Scale (ODS) and Optimal Image Scale (OIS) that provide a metric for the whole dataset.

The Optimal Dataset Scale (ODS), where one chooses the optimal threshold for the entire dataset before applying the F1 score, the Optimal Image Scale (OIS), where one chooses the optimal threshold per-image before using the F1 score, are two metrics to evaluate the quality of edge detection algorithm on the whole dataset. The OIS is always a bit better than the ODS, since it considers the best scale for each image. The OIS corresponds to the optimistic situation where we have the optimal threshold for each image of the dataset. For more information about these classical measures for edge detection, we refer to Arbelaez et al. [2011]Liu et al. [2019].

We can see in Figure 12 examples where RCF has missed to detect edges, and in Figure 13 examples where RCF detect edges while there are no edges. Finally, in Figure 14 we can see some examples where our algorithm fails.

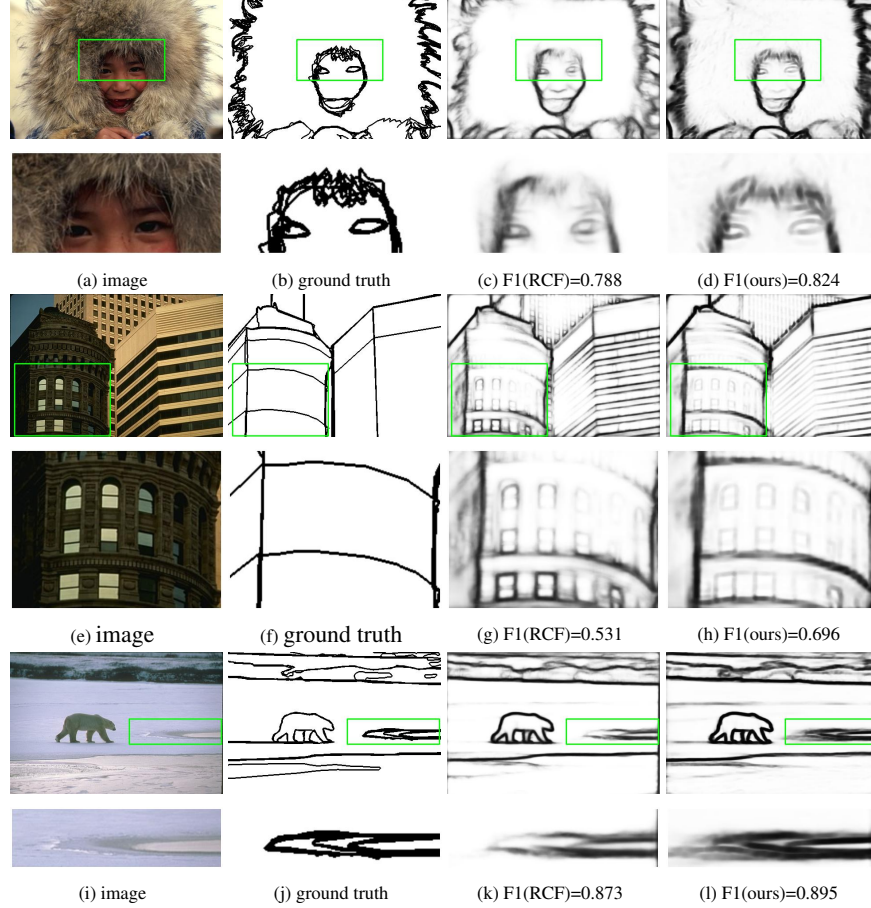


Figure 12: Overview of results of different methods on BSD500Arbelaez et al. [2011].From left to right: original image, ground truth, RCFLiu et al. [2019b] predict edge map, NAO\_multi\_scale predicted edge map. We can see in these examples that RCF has more False Negative than NAO\_multi\_scale.

Method	ODS	OIS	AP	R50
DeepEdge Bertasius et al. [2015a]	0.753	0.772	0.807	
$N^4$ -Fields Ganin and Lempitsky [2014]	0.753	0.767	0.780	
HFL Bertasius et al. [2015b]	0.767	0.788	0.800	
HED Xie and Tu [2015a]	0.782	0.804	0.833	
RDS Liu and Lew [2016]	0.792	0.810		
CEDN Yang et al. [2016]	0.788	0.804		
AMH-Net(fusion) Xu et al. [2018]	0.798	0.829	0.869	
CED Wang et al. [2019]	0.803	0.820	0.871	
MIL+G-DSN+VOC+MS+NCuts Kokkinos [2015]	0.813	<b>0.831</b>		
RCF_ResNet101 Liu et al. [2019b]	0.812	0.829		
<b>NAO-U-NET(ours)</b> with dilation search space	0.788	0.808	0.814	0.899
<b>NAO-Multi-scale(ours)</b> without morphological search space	0.812	0.830	0.827	0.903
<b>NAO-Multi-scale(ours)</b> with dilation search space	$\pm 0.001$	$\pm 0.001$	$\pm 0.014$	$\pm 0.00471$
<b>NAO-Multi-scale(ours)</b> with gradient search space	<b>0.814</b>	<b>0.831</b>	<b>0.850</b>	<b>0.908</b>

Table 5: Performance of NAO\_ResNet and comparison with other competitors on BSD500 test set, measured using the methodXie and Tu [2015b]. For our experiments, the results are presented as mean  $\pm std - dev$  computed from 3 runs.

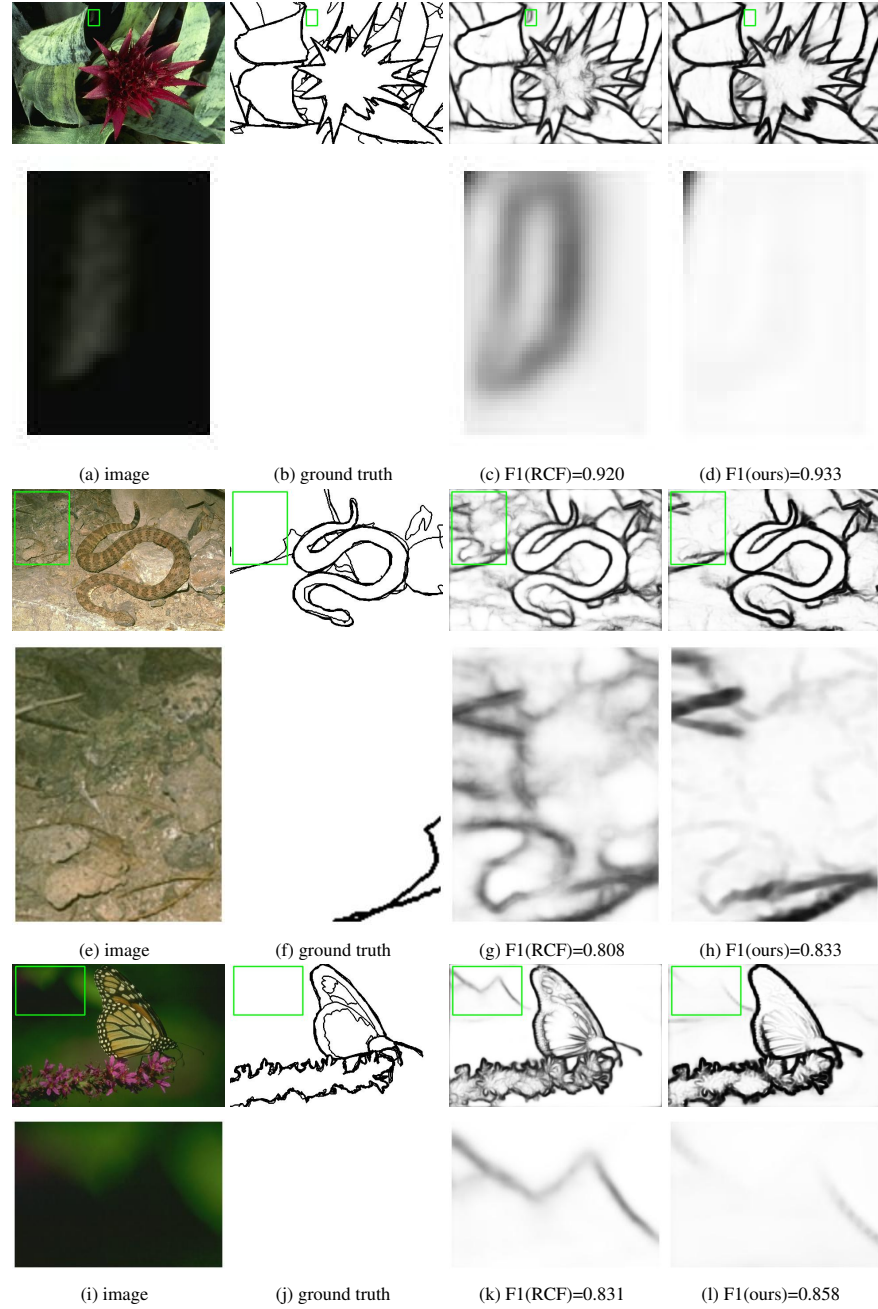


Figure 13: Overview of results of different methods on BSD500Arbelaez et al. [2011].From left to right: original image, ground truth, RCFLiu et al. [2019b] predict edge map, NAO\_multi\_scale predicted edge map. We can see in these examples that RCF has more False Positive than NAO\_multi\_scale.

In Table 5, one can see our results **NAO-Multi-scale** outperforms state-of-the-art results when we use the gradient search space. This comes from the fact that gradient can be used to detect edge detection; hence, using this layer helps the DNN to estimate the edge detection.

### 4.3 Discussions

We demonstrated in prior experiments that morphological layers boost the DNN’s performance for a specific architecture search methodology. However, the improvement is not consistent across all levels. As seen in Table 3 erosion layers perform worse than DNN without morphological layers. However, dilation layers increase performance. This

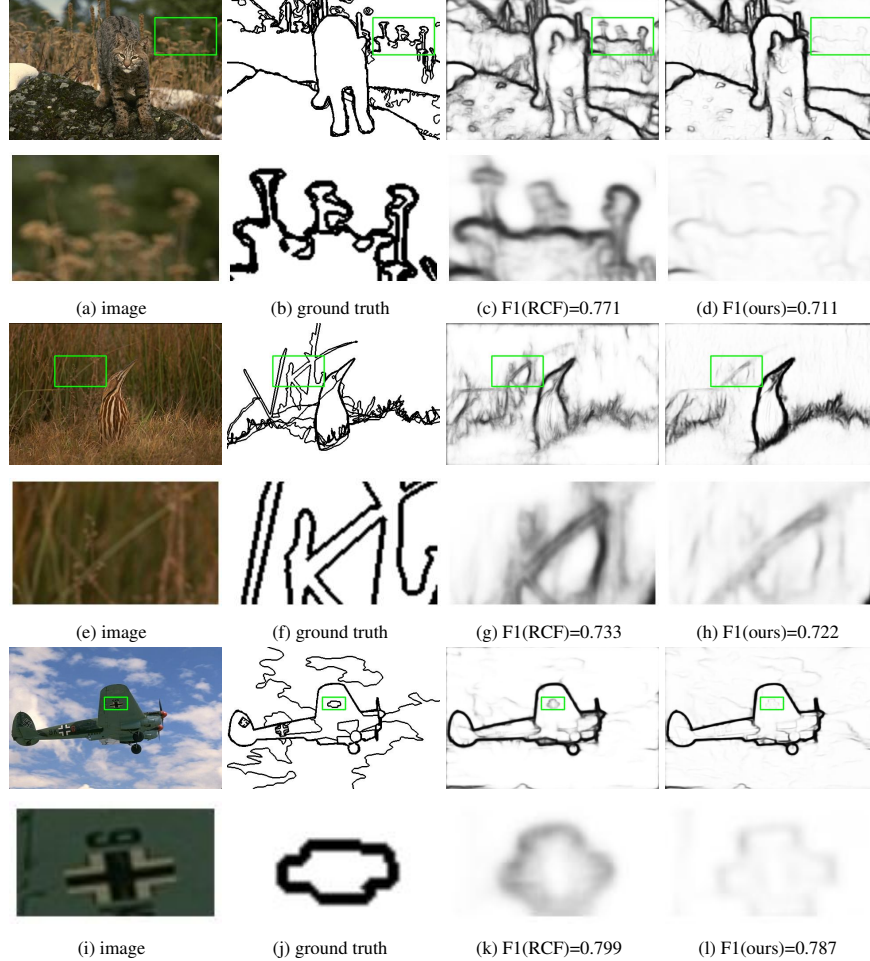


Figure 14: Overview of results of different methods on BSD500Arbelaez et al. [2011].From left to right: original image, ground truth, RCFLiu et al. [2019b] predict edge map, NAO\_multiscale predicted edge map. We can see in these examples that NAO\_multiscale has more False Negatif than RCF.

improvement is due to the fact that erosion is associated with a min-pooling process that extracts the less noticeable region. Similarly, as seen in Table 5, the DNN learned with dilation layers degrades performance, whereas the gradient-based DNN improves it. This brings up one point: if the morphological layers are chosen correctly, they can enhance the representational power of a DNN. Another intriguing element of the edge detection studies is that the search space of the architecture matters, as we observe that the U-Net search space produces lower results than the multi-scale decoder search space that we suggest. As illustrated in Figure 12 and 13 multi-resolution aids in obtaining a better edge since some items may be more easily spotted at specific resolutions than others. Finally, we note that the results obtained using the multi-scale decoder search space with the gradient layer are state-of-the-art. As a result, this demonstrates the use of these layers.

## 5 Conclusion

This paper introduces a new layer for Deep Neural Networks that is based on mathematical morphology. We offer a novel equitable technique for determining the utility of a new layer. This method is applied to our newly created layers. We conclude that our layer has the potential to be extremely useful for image categorization and edge detection. This evaluation methodology appears to be more equitable than the standard approach, which entails proposing a new layer and handcrafting an architecture to increase performance. Everything is optimized using an algorithm in this case.

Additionally, we suggest a new backbone architecture for architecture search. Both the input and output are images, which we refer to as **NAO-Multi-scale**. We compared it to the Unet architecture search and established that our search

architecture outperforms the Unet architecture search. Finally, we achieved state-of-the-art edge detection performance using **NAO-Multi-scale** and gradient operations.

In future research, we will examine how to employ such layers to do semantic segmentation based on these encouraging results. Semantic segmentation is a hot topic, and it will be interesting to watch how it interacts with these morphological levels. Additionally, it will be fascinating to deal with more specialized information, such as remote sensing data containing several photographs of buildings and roads with unique geometric shapes. As such, it may be instructive to observe how these new layers act in this scenario.

## Acknowledgement

We would like to thank CNRS Jean-Zay supercomputer.

## References

Alex Krizhevsky, Ilya Sutskever, and Geoffrey E. Hinton. Imagenet classification with deep convolutional neural networks. In *International Conference on Neural Information Processing Systems*, pages 1097–1105, 2012.

Karen Simonyan and Andrew Zisserman. Very deep convolutional networks for large-scale image recognition. *arXiv preprint arXiv:1409.1556*, 2014a.

Kaiming He, Xiangyu Zhang, Shaoqing Ren, and Jian Sun. Deep residual learning for image recognition. In *Proceedings of the IEEE conference on computer vision and pattern recognition*, pages 770–778, 2016a.

Gao Huang, Zhuang Liu, Laurens Van Der Maaten, and Kilian Q Weinberger. Densely connected convolutional networks. In *Proceedings of the IEEE conference on computer vision and pattern recognition*, pages 4700–4708, 2017.

Joseph Redmon, Santosh Divvala, Ross Girshick, and Ali Farhadi. You only look once: Unified, real-time object detection. In *Proceedings of the IEEE conference on computer vision and pattern recognition*, pages 779–788, 2016.

Zihang Dai, Zhilin Yang, Yiming Yang, William W Cohen, Jaime Carbonell, Quoc V Le, and Ruslan Salakhutdinov. Transformer-xl: Attentive language models beyond a fixed-length context. *arXiv preprint arXiv:1901.02860*, 2019.

Alec Radford, Jeffrey Wu, Rewon Child, David Luan, Dario Amodei, and Ilya Sutskever. Language models are unsupervised multitask learners. *OpenAI Blog*, 1:8, 2019.

Hanxiao Liu, Karen Simonyan, and Yiming Yang. Darts: Differentiable architecture search, 2019a.

Renqian Luo, Fei Tian, Tao Qin, Enhong Chen, and Tie-Yan Liu. Neural architecture optimization, 2019.

Chenxi Liu, Barret Zoph, Maxim Neumann, Jonathon Shlens, Wei Hua, Li-Jia Li, Li Fei-Fei, Alan Yuille, Jonathan Huang, and Kevin Murphy. Progressive neural architecture search. In *Proceedings of the European conference on computer vision (ECCV)*, pages 19–34, 2018.

Hieu Pham, Melody Guan, Barret Zoph, Quoc Le, and Jeff Dean. Efficient neural architecture search via parameters sharing. In *International Conference on Machine Learning*, pages 4095–4104. PMLR, 2018.

Y. Weng, T. Zhou, Y. Li, and X. Qiu. Nas-unet: Neural architecture search for medical image segmentation. *IEEE Access*, 7:44247–44257, 2019. ISSN 2169-3536. doi:10.1109/ACCESS.2019.2908991.

Martin Wistuba, Ambrish Rawat, and Tejaswini Pedapati. A survey on neural architecture search, 2019.

Thomas Elsken, Jan Hendrik Metzen, and Frank Hutter. Neural architecture search: A survey, 2019.

Jean-Francois Rivest, Pierre Soille, and Serge Beucher. Morphological gradients. *Journal of Electronic Imaging*, 2(4): 326–336, 1993.

Jean Serra. Image analysis and mathematical morphology, v. 2. 1988.

Guillaume Thibault, Jesus Angulo, and Fernand Meyer. Advanced statistical matrices for texture characterization: application to cell classification. *IEEE Transactions on Biomedical Engineering*, 61(3):630–637, 2013.

Gianni Franchi and Jesus Angulo. Comparative study on morphological principal component analysis of hyperspectral images. In *2014 6th Workshop on Hyperspectral Image and Signal Processing: Evolution in Remote Sensing (WHISPERS)*, pages 1–4. IEEE, 2014.

Gabriele Cavallaro, Nicola Falco, Mauro Dalla Mura, and Jón Atli Benediktsson. Automatic attribute profiles. *IEEE Transactions on Image Processing*, 26(4):1859–1872, 2017.

Santiago Velasco-Forero and Jesus Angulo. Classification of hyperspectral images by tensor modeling and additive morphological decomposition. *Pattern Recognition*, 46(2):566–577, 2013.

Gianni Franchi and Jesus Angulo. Morphological principal component analysis for hyperspectral image analysis. *ISPRS International Journal of Geo-Information*, 5(6):83, 2016.

Gianni Franchi, Amin Fehri, and Angela Yao. Deep morphological networks. *Pattern Recognition*, 102:107246, 2020. ISSN 0031-3203.

Marcos Eduardo Valle. Reduced dilation-erosion perceptron for binary classification. *Mathematics*, 8(4):512, Apr 2020. ISSN 2227-7390.

Ranjan Mondal, Moni Shankar Dey, and Bhabatosh Chanda. Image restoration by learning morphological opening-closing network. *Mathematical Morphology-Theory and Applications*, 4(1):87–107, 2020.

Alex Krizhevsky. Learning multiple layers of features from tiny images. Technical report, 2009.

D. Martin, C. Fowlkes, D. Tal, and J. Malik. A database of human segmented natural images and its application to evaluating segmentation algorithms and measuring ecological statistics. In *Proc. 8th Int'l Conf. Computer Vision*, volume 2, pages 416–423, July 2001.

Jean Serra. *Image Analysis and Mathematical Morphology*. Academic Press, Inc., Orlando, FL, USA, 1983. ISBN 0126372403.

Marie-Laure Boizeau, Pierre Fons, Lionel Cousseins, Josette Desjober, David Sibrac, Corinne Michaux, Anne-Laure Nestor, Bruno Gautret, Keith Neil, Corentin Herbert, et al. Automated image analysis of in vitro angiogenesis assay. *Journal of laboratory automation*, 18(5):411–415, 2013.

Gianni Franchi, Jesus Angulo, Maxime Moreaud, and Loïc Sorbier. Enhanced edx images by fusion of multimodal sem images using pansharpening techniques. *Journal of microscopy*, 269(1):94–112, 2018.

Sébastien Drouyer, Serge Beucher, Michel Bilodeau, Maxime Moreaud, and Loïc Sorbier. Sparse stereo disparity map densification using hierarchical image segmentation. In *International symposium on mathematical morphology and its applications to signal and image processing*, pages 172–184. Springer, 2017.

Gabriele Cavallaro. *Spectral-Spatial Classification of Remote Sensing Optical Data with Morphological Attribute Profiles using Parallel and Scalable Methods*. PhD thesis, University of Iceland, 2016.

Mathieu Fauvel, Jocelyn Chanussot, Jon Atli Benediktsson, and Johannes R Sveinsson. Spectral and spatial classification of hyperspectral data using svms and morphological profiles. In *2007 IEEE International Geoscience and Remote Sensing Symposium*, pages 4834–4837. IEEE, 2007.

Jon Atli Benediktsson, Martino Pesaresi, and Kolbeinn Amazon. Classification and feature extraction for remote sensing images from urban areas based on morphological transformations. *IEEE Transactions on Geoscience and Remote Sensing*, 41(9):1940–1949, 2003.

Alice Dufour, Christian Ronse, Joseph Baruthio, Olena Tankyevych, Hugues Talbot, and Nicolas Passat. Morphology-based cerebrovascular atlas. In *2013 IEEE 10th International Symposium on Biomedical Imaging*, pages 1210–1214. IEEE, 2013.

Xiwei Zhang, Guillaume Thibault, Etienne Decencière, Gwénolé Quellec, Guy Cazuguel, Ali Erginay, Pascale Massin, and Agnès Chabouis. Spatial normalization of eye fundus images. In *ISBI 2012: 9th IEEE International Symposium on Biomedical Imaging*. IEEE, 2012.

Jonathan Masci, Jesús Angulo, and Jürgen Schmidhuber. A learning framework for morphological operators using counter-harmonic mean. In *International Symposium on Mathematical Morphology and Its Applications to Signal and Image Processing*, pages 329–340. Springer, 2013.

Faraz Saeedan, Nicolas Weber, Michael Goesele, and Stefan Roth. Detail-preserving pooling in deep networks. In *Proceedings of the IEEE Conference on Computer Vision and Pattern Recognition*, pages 9108–9116, 2018.

Yunxiang Zhang, Samy Blusseau, Santiago Velasco-Forero, Isabelle Bloch, and Jesus Angulo. Max-plus operators applied to filter selection and model pruning in neural networks. *arXiv preprint arXiv:1903.08072*, 2019.

Ranjan Mondal, Sanchayan Santra, and Bhabatosh Chanda. Dense morphological network: An universal function approximator. *arXiv preprint arXiv:1901.00109*, 2019.

Vasileios Charisopoulos and Petros Maragos. Morphological perceptrons: geometry and training algorithms. In *International Symposium on Mathematical Morphology and Its Applications to Signal and Image Processing*, pages 3–15. Springer, 2017.

Dorra Mellouli, Tarek M Hamdani, Mounir Ben Ayed, and Adel M Alimi. Morph-cnn: A morphological convolutional neural network for image classification. In *International Conference on Neural Information Processing*, pages 110–117. Springer, 2017.

Keiller Nogueira, Jocelyn Chanussot, Mauro Dalla Mura, William Robson Schwartz, and Jefersson A. dos Santos. An introduction to deep morphological networks, 2019.

Samy Blusseau, Bastien Ponchon, Santiago Velasco-Forero, Jesús Angulo, and Isabelle Bloch. Approximating morphological operators with part-based representations learned by asymmetric auto-encoders. *Mathematical Morphology - Theory and Applications*, 4(1):64 – 86, 01 Jan. 2020.

Marc-André Zöller and Marco F Huber. Survey on automated machine learning. *arXiv preprint arXiv:1904.12054*, 2019.

Marcandre Zoller and Marco F Huber. Benchmark and survey of automated machine learning frameworks. *arXiv: Learning*, 2020.

Barret Zoph and Quoc V Le. Neural architecture search with reinforcement learning. *arXiv preprint arXiv:1611.01578*, 2016.

Dario Floreano, Peter Dürr, and Claudio Mattiussi. Neuroevolution: from architectures to learning. *Evolutionary intelligence*, 1(1):47–62, 2008.

Pengzhen Ren, Yun Xiao, Xiaojun Chang, Po-Yao Huang, Zhihui Li, Xiaojiang Chen, and Xin Wang. A comprehensive survey of neural architecture search: Challenges and solutions, 2020.

Hiroaki Kitano. Designing neural networks using genetic algorithms with graph generation system. *Complex systems*, 4 (4):461–476, 1990.

Geoffrey F Miller, Peter M Todd, and Shailesh U Hegde. Designing neural networks using genetic algorithms. In *ICGA*, volume 89, pages 379–384, 1989.

Yun Liu, Ming-Ming Cheng, Xiaowei Hu, Jia-Wang Bian, Le Zhang, Xiang Bai, and Jinhui Tang. Richer convolutional features for edge detection. *IEEE Transactions on Pattern Analysis and Machine Intelligence*, 41(8):1939–1946, Aug 2019b. ISSN 1939-3539.

Andrés Camero, Hao Wang, Enrique Alba, and Thomas Bäck. Bayesian neural architecture search using a training-free performance metric. *arXiv preprint arXiv:2001.10726*, 2020.

Jesus Angulo. Convolution in (max,min)-algebra and its role in mathematical morphology. In *Advances in imaging and electron physics*, volume 203, pages 1–66. Elsevier, 2017.

Pablo Arbelaez, Michael Maire, Charless Fowlkes, and Jitendra Malik. Contour detection and hierarchical image segmentation. *IEEE Trans. Pattern Anal. Mach. Intell.*, 33(5):898–916, May 2011. ISSN 0162-8828.

Wenzhe Shi, Jose Caballero, Ferenc Huszár, Johannes Totz, Andrew P. Aitken, Rob Bishop, Daniel Rueckert, and Zehan Wang. Real-time single image and video super-resolution using an efficient sub-pixel convolutional neural network, 2016.

Sergey Ioffe and Christian Szegedy. Batch normalization: Accelerating deep network training by reducing internal covariate shift. In *International conference on machine learning*, pages 448–456. PMLR, 2015.

Kaiming He, Xiangyu Zhang, Shaoqing Ren, and Jian Sun. Deep residual learning for image recognition. In *Proceedings of the IEEE conference on computer vision and pattern recognition*, pages 770–778, 2016b.

Karen Simonyan and Andrew Zisserman. Very deep convolutional networks for large-scale image recognition. *arXiv preprint arXiv:1409.1556*, 2014b.

Christian Szegedy, Sergey Ioffe, Vincent Vanhoucke, and Alexander Alemi. Inception-v4, inception-resnet and the impact of residual connections on learning. In *Proceedings of the AAAI Conference on Artificial Intelligence*, volume 31, 2017.

Barret Zoph, Vijay Vasudevan, Jonathon Shlens, and Quoc V Le. Learning transferable architectures for scalable image recognition. In *Proceedings of the IEEE conference on computer vision and pattern recognition*, pages 8697–8710, 2018.

François Chollet. Xception: Deep learning with depthwise separable convolutions. In *Proceedings of the IEEE conference on computer vision and pattern recognition*, pages 1251–1258, 2017.

Olaf Ronneberger, Philipp Fischer, and Thomas Brox. U-net: Convolutional networks for biomedical image segmentation, 2015.

Liang-Chieh Chen, Yukun Zhu, George Papandreou, Florian Schroff, and Hartwig Adam. Encoder-decoder with atrous separable convolution for semantic image segmentation. In *Proceedings of the European conference on computer vision (ECCV)*, pages 801–818, 2018.

Hengshuang Zhao, Jianping Shi, Xiaojuan Qi, Xiaogang Wang, and Jiaya Jia. Pyramid scene parsing network. In *Proceedings of the IEEE conference on computer vision and pattern recognition*, pages 2881–2890, 2017.

Olga Russakovsky, Jia Deng, Hao Su, Jonathan Krause, Sanjeev Satheesh, Sean Ma, Zhiheng Huang, Andrej Karpathy, Aditya Khosla, Michael Bernstein, Alexander C. Berg, and Li Fei-Fei. Imagenet large scale visual recognition challenge, 2015.

Gao Huang, Yu Sun, Zhuang Liu, Daniel Sedra, and Kilian Weinberger. Deep networks with stochastic depth, 2016.

Sergey Zagoruyko and Nikos Komodakis. Wide residual networks, 2017.

Zhao Zhong, Junjie Yan, Wei Wu, Jing Shao, and Cheng-Lin Liu. Practical block-wise neural network architecture generation, 2018.

Gao Huang, Zhuang Liu, Laurens van der Maaten, and Kilian Q. Weinberger. Densely connected convolutional networks, 2018.

Yu Liu and Michael S Lew. Learning relaxed deep supervision for better edge detection. In *Proceedings of the IEEE conference on computer vision and pattern recognition*, pages 231–240, 2016.

Jimei Yang, Brian Price, Scott Cohen, Honglak Lee, and Ming-Hsuan Yang. Object contour detection with a fully convolutional encoder-decoder network. In *Proceedings of the IEEE conference on computer vision and pattern recognition*, pages 193–202, 2016.

Iasonas Kokkinos. Pushing the boundaries of boundary detection using deep learning. *arXiv preprint arXiv:1511.07386*, 2015.

Roozbeh Mottaghi, Xianjie Chen, Xiaobai Liu, Nam-Gyu Cho, Seong-Whan Lee, Sanja Fidler, Raquel Urtasun, and Alan Yuille. The role of context for object detection and semantic segmentation in the wild. In *Proceedings of the IEEE Conference on Computer Vision and Pattern Recognition*, pages 891–898, 2014.

Changbao Wen, Pengli Liu, Wenbo Ma, Zhirong Jian, Changheng Lv, Jitong Hong, and Xiaowen Shi. Edge detection with feature re-extraction deep convolutional neural network. *Journal of Visual Communication and Image Representation*, 57:84 – 90, 2018. ISSN 1047-3203.

Y. Liu, M. Cheng, X. Hu, J. Bian, L. Zhang, X. Bai, and J. Tang. Richer convolutional features for edge detection. *IEEE Transactions on Pattern Analysis and Machine Intelligence*, 41(8):1939–1946, 2019. doi:10.1109/TPAMI.2018.2878849.

Gedas Bertasius, Jianbo Shi, and Lorenzo Torresani. Deepedge: A multi-scale bifurcated deep network for top-down contour detection. In *Proceedings of the IEEE Conference on Computer Vision and Pattern Recognition*, pages 4380–4389, 2015a.

Yaroslav Ganin and Victor Lempitsky.  $n^4$ -fields: Neural network nearest neighbor fields for image transforms, 2014.

Gedas Bertasius, Jianbo Shi, and Lorenzo Torresani. High-for-low and low-for-high: Efficient boundary detection from deep object features and its applications to high-level vision, 2015b.

Saining Xie and Zhuowen Tu. Holistically-nested edge detection, 2015a.

Dan Xu, Wanli Ouyang, Xavier Alameda-Pineda, Elisa Ricci, Xiaogang Wang, and Nicu Sebe. Learning deep structured multi-scale features using attention-gated crfs for contour prediction, 2018.

Yupei Wang, Xin Zhao, Yin Li, and Kaiqi Huang. Deep crisp boundaries: From boundaries to higher-level tasks. *IEEE Transactions on Image Processing*, 28(3):1285–1298, Mar 2019. ISSN 1941-0042.

Saining Xie and Zhuowen Tu. Holistically-nested edge detection. In *Proceedings of the IEEE international conference on computer vision*, pages 1395–1403, 2015b.